IEEE Photonics Journal
An IEEE Photonics Society Publication

Open Access

A 1 × *N* Lossless Adaptive Optical Power Splitter Employing an Opto-VLSI Processor

Volume 5, Number 6, December 2013

Haithem A. B. Mustafa
Feng Xiao
Kamal Alameh

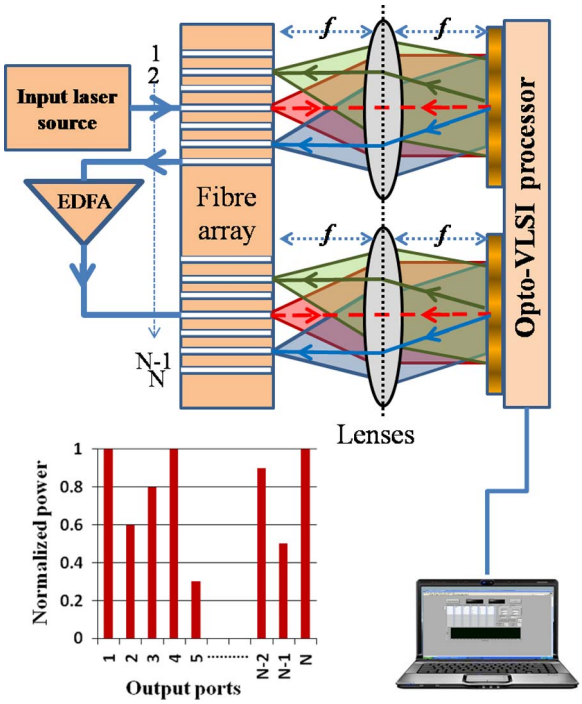

DOI: 10.1109/JPHOT.2013.2285718
1943-0655 © 2013 IEEE

IEEE photonics SOCIETY

IEEE

A 1 × *N* Lossless Adaptive Optical Power Splitter Employing an Opto-VLSI Processor

Haithem A. B. Mustafa, Feng Xiao, and Kamal Alameh

Electron Science Research Institute, Edith Cowan University, Joondalup, WA 6027, Australia

DOI: 10.1109/JPHOT.2013.2285718

Manuscript received August 15, 2013; revised September 27, 2013; accepted September 28, 2013. Date of current version October 25, 2013. Corresponding author: H. A. B. Mustafa (e-mail: hmustafa@student.ecu.edu.au).

Abstract: We propose and demonstrate the concept of a novel 1 × *N* lossless adaptive optical power splitter (OPS) structure integrating a software-driven Opto-VLSI processor, optical amplifiers, and an array of 4-f imaging systems. The active area of the Opto-VLSI processor is divided into *M* pixel blocks driven by multicasting phase holograms and aligned with an *M*-element lens array and a fiber array, thus forming an array of 4-f imaging systems. Each 4-f imaging system is capable of collimating and adaptively splitting an input optical beam emerging from an optical fiber and then coupling the split beams into different output fiber ports, thus realizing dynamic optical power splitting. The Opto-VLSI processor is driven by optimized multicasting phase holograms that adaptively split an incident laser beam along different angles; thus, user-defined splitting ratios can be achieved. Experimental results show that the optical amplifiers compensate for the splitting and the insertion losses, making the adaptive OPS lossless.

Index Terms: Adaptive optical splitter, beam splitter, liquid crystal devices, optical communications, Opto-VLSI processor.

1. Introduction

Adaptive optical power splitters (OPSs) are used in many applications, including passive optical networks (PON) and photonic RF signal processing [1], [2]. In PONs such as fiber-to-the-premise (FTTP), adaptive optical splitters enable the power in a fiber optical network to be distributed more efficiently to subscribers, thus making fiber-to-the-home services cost effective [3]. Adaptive OPS can also improve the optical network scalability by actively delivering optical signals according to the users' demand [4]. An adaptive OPS can also be used in double fiber ring PONs for realizing self-healing ring-to-ring optical metropolitan area networks (MAN) [5], thus offering automatic communication recovery when line break occurs. In addition, future optical line protection (OLP) systems require adaptive optical splitters to i) switch optical signals from faulty lines to active power lines, ii) avoid the use of optical attenuators and/or amplifiers, and iii) real time line monitoring [6]. Adaptive OPSs also enable optical networks to be more flexible and scalable [7].

The research area of photonic RF signals processing benefits particularly from the development of adaptive OPSs especially because of their lightweight and broadband features [8], [9]. For example, an adaptive OPS can add a new feature to a tunable photonic microwave filter by adaptively changing the filter weights [10]–[12]. An adaptive OPS can also be used to dynamically split an RF-modulated optical signal into numerous output ports, thus realizing a broadband adaptive RF power splitter [13].

Several adaptive OPS technologies have been reported based on tuned fiber Bragg gratings (FBGs) [14], optical polarization splitters [15], semiconductor optical amplifiers [16], [17], waveguide

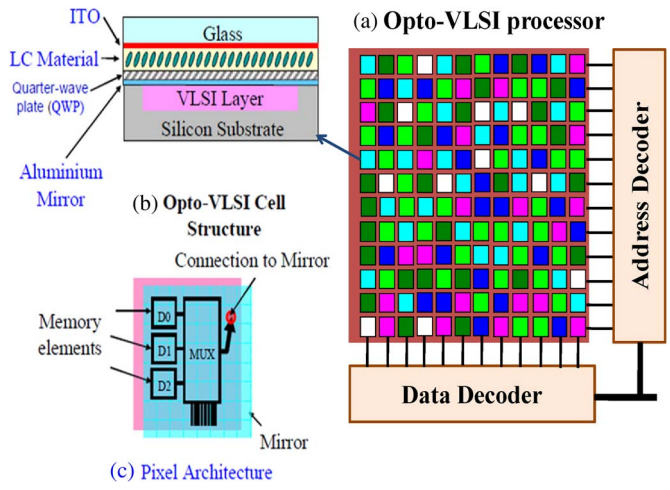

Fig. 1. (a) Opto-VLSI processor layout, (b) cell structure, and (c) pixel architecture.

couplers and planar lightwave circuits (PLCs) [18]–[20], MEMS [21], and Opto-VLSI [22]–[24]. However, these techniques have limited tolerance to environmental perturbations, high polarization dependence, and limited numbers of output ports.

The key features of a practical OPS include the insertion loss, output port count, size and cost. The authors have recently reported an adaptive optical splitter structure based on the use of an Opto-VLSI processor in combination with a fiber collimator array and single-lens 4-f imaging system [23]. The number of output ports for this structure was limited to two ports because the spacing of the fiber collimator array was large (3 mm), thus requiring a large beam steering angle which increases the insertion loss. To eliminate the need for large steering angles, the authors replaced the fiber collimator array with a fiber array with 250 μm fiber-to-fiber spacing [24]. This approach doubled the output port count; however, with the use of a single-lens 4-f imaging system, further increase in the output port count was impractical, due to the high insertion loss experienced by the split optical beams routed to the outer fiber ports, which require large beam steering angles for optimum beam coupling.

In this article, we propose and demonstrate the principle of a novel $1 \times N$ lossless adaptive optical splitter structure integrating an Opto-VLSI processor, fiber array and an array of 4-f imaging systems (employing an array of lenslets rather than a single lens). The proposed splitter structure enables an input optical power to be split adaptively into a much larger number of output fiber ports compared to previously reported structures, through optimized phase holograms driving the Opto-VLSI processor. The new adaptive optical splitter has additional advantages including lossless operation, adequate inter-port crosstalk, compressed hardware and simple user interface.

2. Opto-VLSI Processor and Optical Beam Multicasting

The Opto-VLSI processor, also known as spatial light modulator (SLM), is an electronically-driven, motionless diffractive element that can steer/reshape an incident laser beam. Illustrated in Fig. 1, an Opto-VLSI processor incorporates an array of liquid crystal (LC) cells addressed by a Very-Large-Scale-Integrated (VLSI) circuit [23], [24] that generates phase holograms capable of arbitrary steering and/or multicasting input laser beams. By depositing a quarter-wave-plate (QWP) layer between the LC layer and the aluminum mirror, polarization-insensitive operation can be accomplished [25]. Also, the use of a transparent Indium-Tin Oxide (ITO) layer as a ground electrode minimizes the optical insertion loss of the Opto-VLSI processor. The voltage of each pixel can individually be adjusted using memory elements that can select a voltage level and apply it, through both electrodes, across each LC cell.

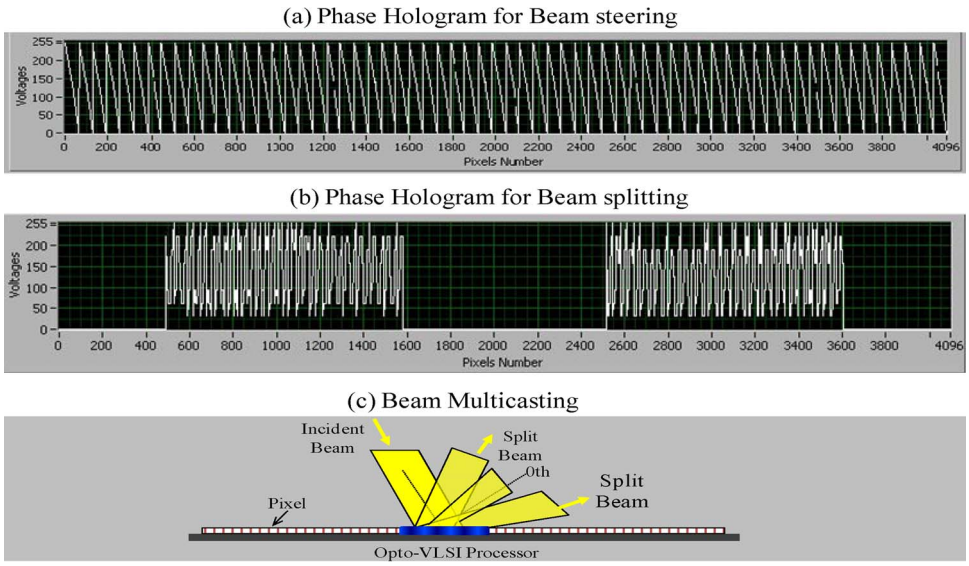

Fig. 2. (a) Typical phase hologram (periodic saw-tooth phase profile) for steering an optical beam. (b) Two typical phase holograms for splitting two incident optical beams. (c) Beam multicasting through the use of a multicasting phase hologram.

Fig. 2 illustrates the capability of a multicasting phase hologram to split an incident laser beam to N output beams with variable intensities along different directions. A collimated light beam incident onto the Opto-VLSI processor is typically diffracted along different directions, and the intensity of each diffracted light beam depends on the multicasting phase hologram. The multicasting angle resolution, or minimum splitting angle relative to the zeroth-order diffraction beam, is expressed as [26]

$$\alpha = \arcsin\left(\frac{\lambda}{N \times d}\right) \tag{1}$$

where λ is the laser wavelength of the incident optical beam, N is representing the quantized nature of the steering/splitting angle by including the number of illuminated pixels, and d is the pixel pitch.

Several computer algorithms, including, genetic, simulated annealing, phase encoding, and projection algorithms [27], have conventionally been used for generating optimized multicasting phase holograms that produce a desired far-field distribution, defined by the beam directions and their intensities.

3. Lossless Adaptive OPS Architecture

Fig. 3 illustrates the concept of the proposed $1 \times N$ lossless adaptive OPS, which comprises an Opto-VLSI processor, a fiber array, a lens array, and Erbium-Doped Fiber Amplifiers (EDFAs). The active area of the Opto-VLSI processor is divided into M pixel-blocks driven by multicasting phase holograms and aligned with an M-element lens array and a fiber array, thus forming an array of 4-f imaging systems. Each 4-f imaging system collimates and adaptively splits an input optical beam launched into the input optical fiber port and then couples the split beams into different output fiber ports, thus realizing a variable OPS. A laser signal is typically launched into the input fiber port (Master block), split into P output optical signals via the uploaded multicasting phase hologram, and then coupled into P output fiber ports. Each output optical signal emerging from each output port is amplified by an EDFA to compensate for the various insertion and splitting losses. Each amplified optical signal is then launched into another input fiber port and adaptively split via another multicasting phase hologram uploaded onto another pixel block dedicated to adaptively split that amplified optical signal.

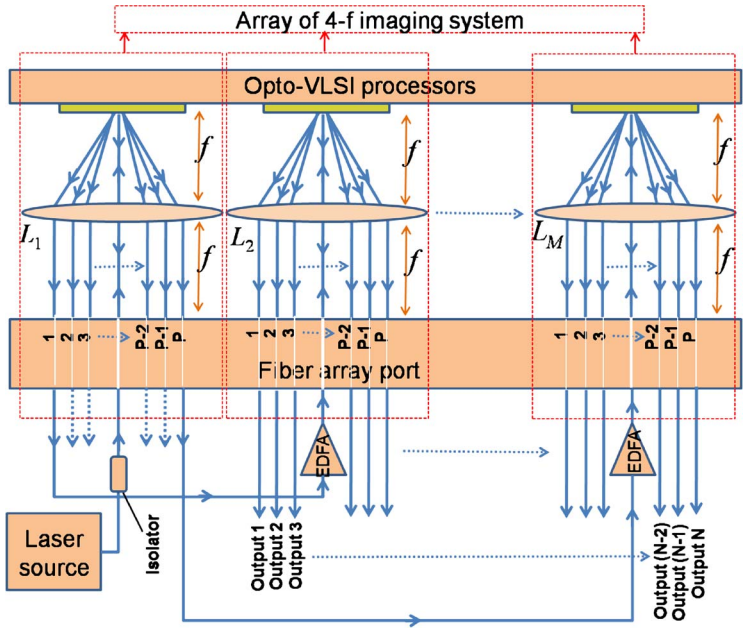

Fig. 3. Schematic diagram of the proposed $1 \times N$ lossless adaptive optical power splitter employing an Opto-VLSI processor, optical amplifiers, and an array of 4-f imaging systems.

The role of the software-driven Opto-VLSI processor is to adaptively split an incident light beam into many different angles, with user-defined splitting ratios, by uploading optimized multicasting phase holograms onto the various pixel blocks. By driving a pixel-block with an optimized multicasting phase hologram, each incident 'input' optical beam illuminating that pixel block can be split into P different optical beams. These split beams propagate along appropriate directions and couple back into the output fiber ports through the corresponding 4-f imaging system. For M pixel-blocks, each splits its input optical beam into P. beams; the total number of the output fiber ports that can be attained is $N = (M - 1) \times P$.

4. Experimental Results and Discussion

To demonstrate the concept of the proposed $1 \times N$ lossless adaptive OPS, several experiments were carried out. Fig. 4(a) shows the first experiment, which was set up to align the various optical components of the splitter. The splitter demonstrator consisted of an Opto-VLSI processor, a 2-element lens array with adjustable lens spacing, and a 1×64 optical fiber array. All components were aligned to form two 4-f imaging systems, as shown in Fig. 4(a). The Opto-VLSI processor used in the experiments has 1×4096 pixels, a pixel size of 1.0 μm $\times$ 6.0 mm, a pixel pitch of 1.8 μm (i.e., 0.8 μm of dead space between pixels), and an active area of 7.4 mm $\times$ 6.0 mm. A fiber array of spacing 127 μm was used as the input/output fiber ports. The lens array had two elements, each of focal length (f) 9 mm and diameter 3 mm, and was placed right at the middle of distance, f, between the Opto-VLSI processor and the fiber array. Two input fiber ports separated by a span of 29 fiber elements (i.e., 29×0.127 mm $= 3.68$ mm) were used to launch two input optical signals of similar intensities. The measured laser power spectral density launched into one of the input fiber ports is shown in Fig. 4(b). The gap between the two lenses was 0.68 mm (properly adjusted to match the spacing between the two input fiber ports). Both input optical signals were collimated through the corresponding lenses, at a diameter of 1.962 mm.

The measured power densities of the input optical beams after collimation by the lens array are shown in Fig. 4(c). Each collimated beam illuminated around 1090 pixels of the Opto-VLSI processor, thus attaining a high diffraction efficiency and high optical splitting angle resolution [23]. The

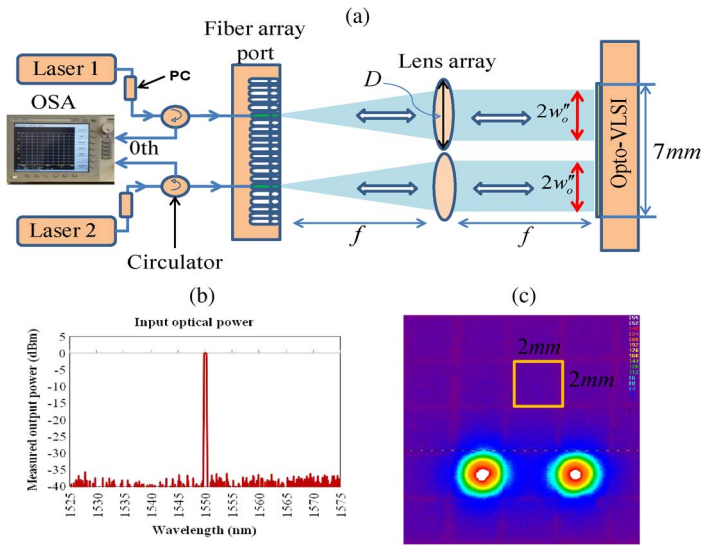

Fig. 4. (a) Experimental setup used to demonstrate the concept of the proposed $1 \times N$ lossless adaptive optical power splitter. (b) Measured laser power spectrum launched into one of the input fiber ports. (c) Measured power densities of the two input optical beams after collimation by the lens array.

active area of the Opto-VLSI processor was divided into two pixel-blocks, separated by 934 unaddressed pixels to avoid beams interference.

A Labview program was especially implemented to generate optimized multicasting phase holograms that split the two input optical beams along different directions, and the split beams were coupled into the various output fiber ports. The diffraction efficiency of the Opto-VLSI processor was measured by monitoring the zeroth order diffracted beams for the input signals coupled to their corresponding fiber ports and routed via optical circulators to an optical spectrum analyzer (OSA), as illustrated in Fig. 4(a).

To demonstrate the capability of the proposed $1 \times N$ lossless adaptive OPS to adaptively split an input optical signal into several output signals and couple them into different fiber ports, another experiment was set up, as illustrated in Fig. 5. Two identical laser signals were launched into the input fiber ports 1 and 2, and two multicasting phase holograms were uploaded onto the Opto-VLSI processor to adaptively split the input optical beams and route the split optical beams, through the 4-f imaging system, to the appropriate output fiber ports. Without a phase hologram uploaded onto each pixel-block of the Opto-VLSI processor, only the zero's order diffraction beams were reflected back and focused through the 4-f imaging systems into the same input optical fiber ports. The steering angle for each split optical beam was within the maximum steering angle of the Opto-VLSI processor ($\pm 3.4^\circ$ with respect to the zeroth order beam direction).

As shown in Fig. 5(b), two identical (1550 nm) laser sources with an output optical power of $+3.6$ dBm were used to launch an input signal via optical circulators into the two input fiber ports of the adaptive OPS. The measured power levels of the zeroth order coupled back into the input fiber ports were similar (~ -1.2 dBm). For both input optical beams, the split optical beams propagated along $\pm 0.81^\circ$, $\pm 1.62^\circ$, $\pm 2.43^\circ$, and $\pm 3.24^\circ$ with respect to the direction of the zeroth order beam. Split beams at $\pm 3.24^\circ$ displayed high insertion loss since they are close to the maximum steering angles ($\pm 3.4^\circ$) of the Opto-VLSI processor [28]. However, an Opto-VLSI processor with larger steering angles will allow more split beams to be coupled to the corresponding output ports.

Several splitting scenarios were experimentally investigated to demonstrate the capability of the proposed OPS to adaptively split an input optical signal. Fig. 6 shows the measured output power levels at the output ports for different splitting ratio profiles. For each desired splitting ratio profile, optimized multicasting phase holograms were synthesized (using simulated annealing algorithms [23]) and uploaded onto the Opto-VLSI processor. As shown in Fig. 6, while the

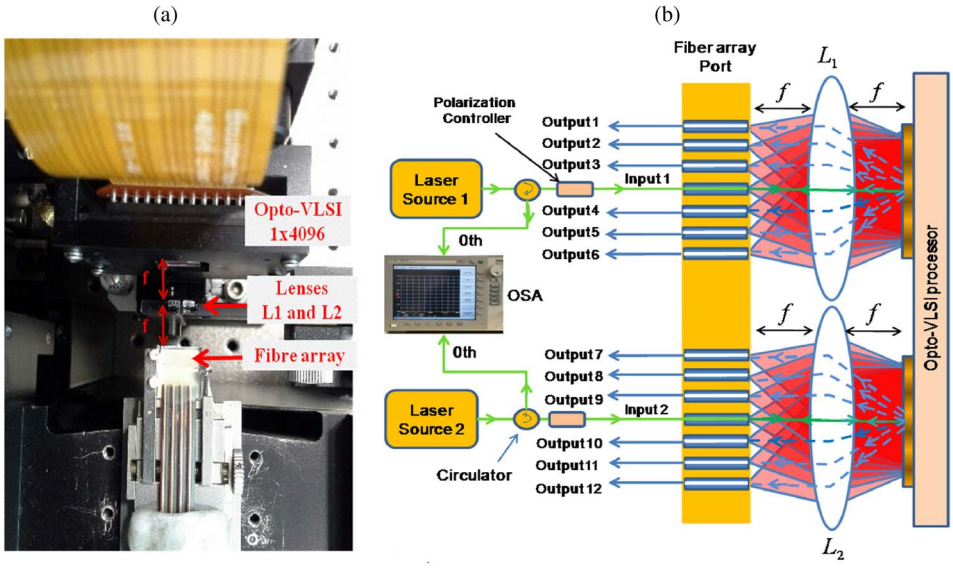

Fig. 5. Experimental setup used to demonstrate the capability of the proposed $1 \times N$ lossless adaptive optical power splitter to adaptively split an input optical signal into several output signals and couple them into different fiber ports. (a) Top view the experimental setup. (b)Two identical laser signals were launched into the input fiber ports, and two multicasting phase holograms were uploaded onto the Opto-VLSI processor to adaptively split the input optical beams and route the split optical beams, through the 4-f imaging system, to the appropriate output fiber ports.

generated multicasting hologram can accurately split the input optical signal and route to the output ports, the crosstalk level was, for some splitting scenarios, relatively high (~ -20 dB). In order to reduce the crosstalk to below -25 dB, tone can intentionally introduce additional very small split signals and route them to other unused output ports, thus reshaping the crosstalk power distribution and avoiding the crosstalk beams to be routed along the intended split beam directions [27].

Fig. 6(a) shows the split signals for Scenario 1, where a multicasting hologram that corresponds to a splitting profile $H1 = 1.0 : 1.0 : 1.0 : 1.0 : 1.0 : 1.0$ was used. Fig. 6(a) demonstrates that the input optical power can be split equally into the output ports, resulting in uniform optical power distribution at all the output ports. Fig. 6(b) shows the split signals for Scenario 2, where a multicasting hologram corresponds to a splitting profile $H2 = 1.0 : 1.0 : 1.0 : 1.0 : 1.0 : 0.2$ was used, which corresponds to the case where the output signals in Ports 6 and 12 were attenuated by 8 dB. Fig. 6(c) shows the split signals for Scenario 3, where a multicasting hologram corresponds to a splitting profile $H3 = 0.2 : 0.5 : 1.0 : 0.2 : 1.0 : 0.2$ was used. For this scenario, the input optical power was arbitrarily split into the output ports, and the theoretical and experimental results are in excellent agreement for all the output fiber ports. Fig. 6(d) shows the split signals for Scenario 4. The signals coupled into Ports 1, 6, 7, and 12 were switched off (highly attenuated), while the signals coupled into Ports 4 and 10 were attenuated by only 4.5 dB, using a phase hologram corresponding to a splitting profile $H4 = 0.0 : 1.0 : 1.0 : 0.3 : 1.0 : 0.0$. For this scenario, the measured crosstalk level was around -25 dB.

Fig. 6 demonstrates the ability of the $1 \times N$ lossless adaptive OPS structure to realize arbitrary optical splitting ratios through the use of optimized multicasting phase holograms. It is important to notice that it is always possible to tailor the splitting profile in order to compensate for the slight misalignment of the optical components as well as the non-uniform fiber spacing of the fiber array.

To demonstrate the lossless operation of the $1 \times N$ lossless adaptive OPS, another experimental setup was used, which is shown in Fig. 7. A laser signal was launched into the input fiber Port 1 and split into six optical signals using a multicasting phase hologram uploaded onto the corresponding

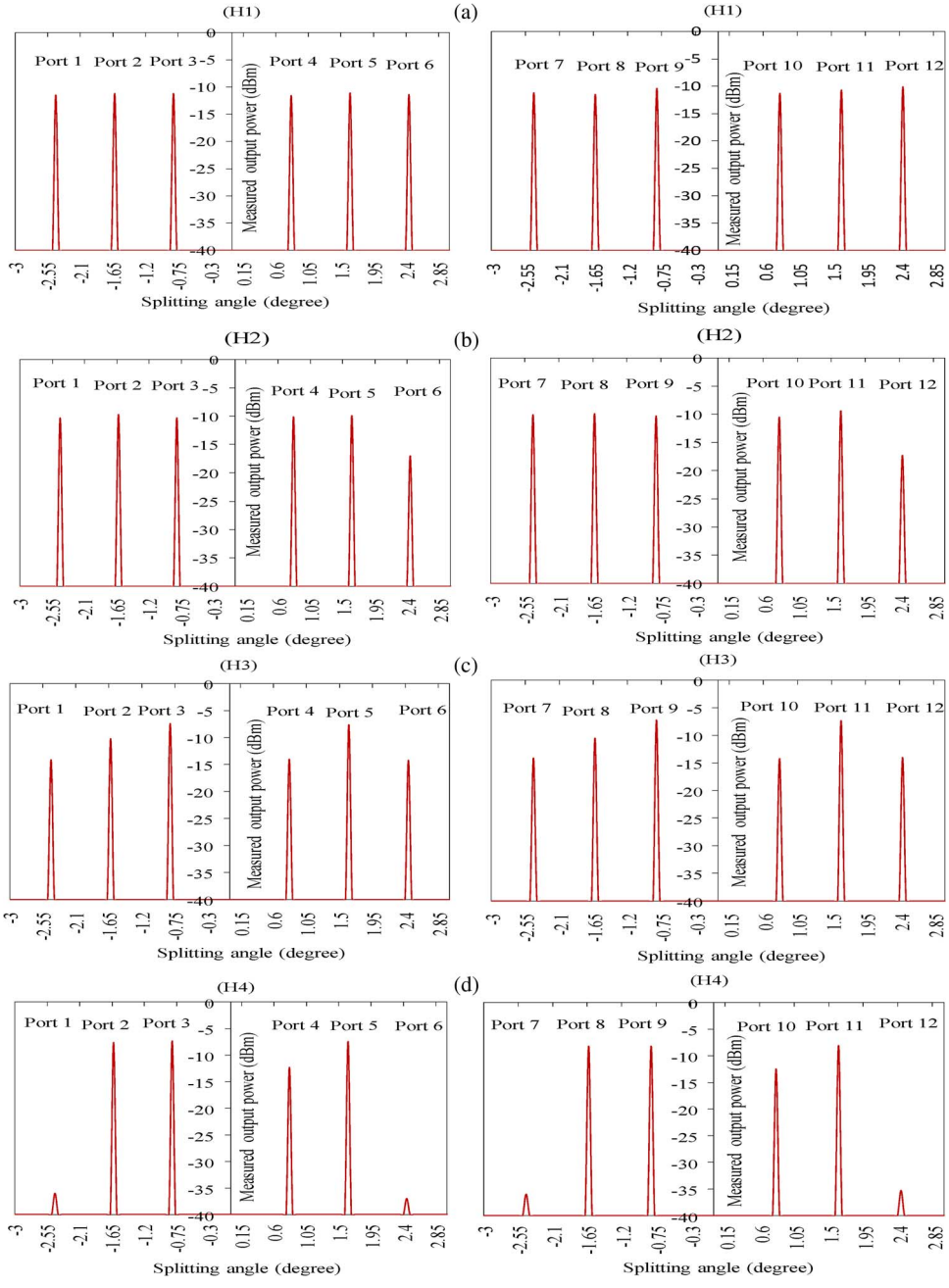

Fig. 6. Measured output power levels at the output ports (1-6 and 7-12) when the two input signals (input 1 and input 2) were split via a multicasting phase hologram corresponding to the splitting profile. (a) H1 = 1.0 : 1.0 : 1.0 : 1.0 : 1.0 : 1.0. (b) H2 = 1.0 : 1.0 : 1.0 : 1.0 : 1.0 : 0.2. (c) H3 = 0.2 : 0.5 : 1.0 : .2 : 1.0 : 0.2. (d) H4 = 0.0 : 1.0 : 1.0 : 0.3 : 1.0 : 0.0.

input pixel block. The sixth split beam was then amplified via an EDFA to compensate for the various insertion and splitting losses of the first splitting stage and then launched into another input fiber port and adaptively split via another multicasting phase hologram uploaded onto another pixel block dedicated to adaptively split that amplified optical signal.

Fig. 8(a)–(c) shows the measured optical power levels coupled into the output fiber ports 7-12 for different multicasting phase holograms uploaded into the Opto-VLSI processor, corresponding to splitting ratio profiles H5 = 0.05 : 0.3 : 0.05 : 0.3 : 1.0 : 0.05, H6 = 0.1 : 0.3 : 1.0 : 1.0 : 0.3 : 0.2,

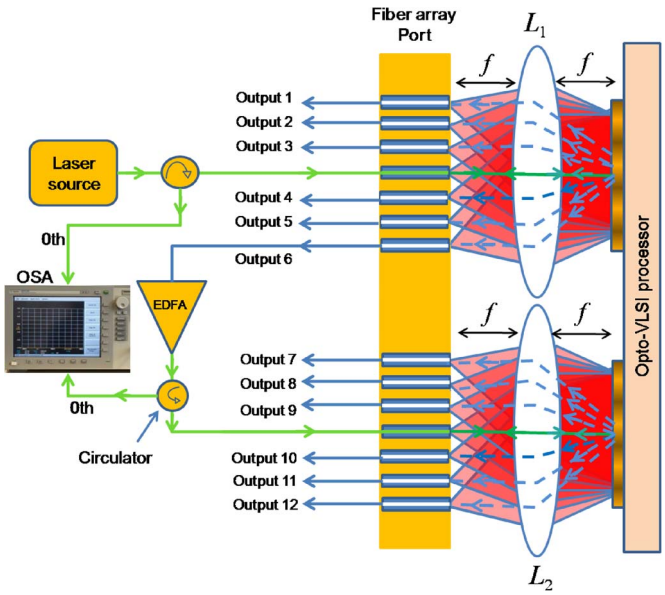

Fig. 7. Experimental setup used to demonstrate the concept of the proposed lossless $1 \times N$ lossless adaptive optical power splitter. A laser signal was launched into the input fibre Port 1 and split using a multicasting phase hologram into six optical signals and then coupled into six output fiber ports. The output signal emerging from port 6 was amplified via EDFA to compensate for the various insertion and splitting losses. The amplified signal was launched into the fiber input Port 2 to undergo subsequent adaptive splitting via another multicasting phase hologram uploaded onto another pixel block dedicated to adaptively split that input signal.

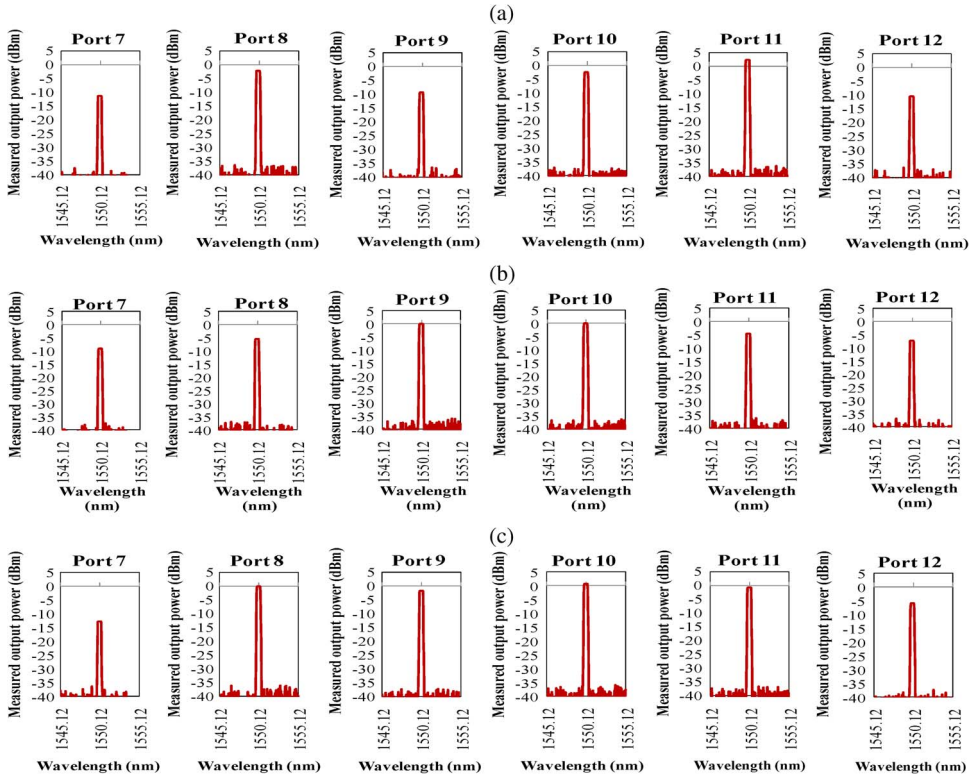

Fig. 8. Measured optical power coupled into the output fiber Ports 7-12 for different multicasting phase holograms corresponding to the following splitting profiles. (a) H5 = 0.05 : 0.3 : 0.05 : 0.3 : 1.0 : 0.05. (b) H6 = 0.1 : 0.3 : 1.0 : 1.0 : 0.3 : 0.2. (c) H7 = 0.05 : 1.0 : 0.6 : 1.0 : 1.0 : 0.3.

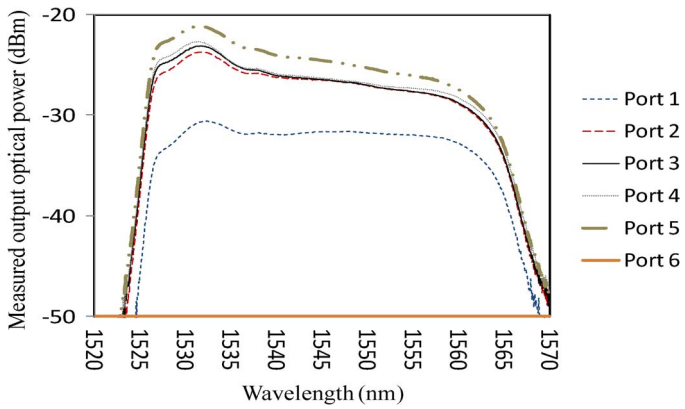

Fig. 9. Measured optical spectra at Ports 1-6 of the adaptive optical power splitter for a splitting profile corresponding to H8 = 0.4 : 0.8 : 0.8 : 0.8 : 1.0 : 0.0. A broadband optical signal replaced the input laser source 1 of Fig. 5.

and H7 = 0.05 : 1.0 : 0.6 : 1.0 : 1.0 : 0.3, respectively. In Fig. 8(a), it is shown that an output optical signal power (Port 11) can be even higher than the input laser power.

Fig. 8(b) and (c) shows that some output optical signals have power levels higher or equal to the power of the input laser, demonstrating the capability of the adaptive OPS to compensate for the various optical losses. It is important to mention that the higher the saturated output optical power of the EDFA, the higher the splitter port count that can be used.

Figs 7 and 8 demonstrate the ability of the proposed $1 \times N$ lossless adaptive OPS structure to realize arbitrary optical splitting ratios through the use of optimized multicasting phase holograms and attain lossless operation.

To measure the spectral bandwidth of the proposed optical splitter, the output of a broadband light source, whose spectra range extends from 1525 nm to 1575 nm, was launched into the input fiber port (Port 5). The measured optical spectra at Ports 1-6 are shown in Fig. 9, for a splitting ratio H8 = 0.4 : 0.8 : 0.8 : 0.8 : 1.0 : 0.0. The measured maximum output power fluctuation for the output ports was around 1.0 dB over a wavelength span from 1525 to 1570 nm, demonstrating a splitter bandwidth in excess of 40 nm.

The total insertion loss of a single 4-f imaging system, without EDFA compensation, was around 4.8 dB, mainly due to the Opto-VLSI processor (3 dB due to it is low fill factor), 4-f optical circulator (1 dB), optical misalignment, and imperfect optical components used in the experiments ($\sim$0.8 dB). Note that the total insertion loss can be reduced through an improved Opto-VLSI chip design with a smaller dead space between pixels and by using broadband antireflection coatings for the key optical components.

5. Conclusion

A $1 \times N$ lossless adaptive OPS structure, integrating Opto-VLSI processor, optical amplifiers, a fiber array, and an array of 4-f imaging systems, has been proposed, and its concept has been experimentally demonstrated. Experimental results have shown that an input optical signal can arbitrarily be split and coupled into 12 output optical fiber ports by simply uploading optimized multicasting phase holograms onto two pixel-blocks of the Opto-VLSI processor. Excellent agreement between theoretical and experimental results has been demonstrated. Results have also shown that the optical amplifiers can compensate for the insertion and splitting losses, thus enabling lossless splitter operation. A crosstalk level around -25 dB and a wavelength spectral range exceeding 40 nm have experimentally been measured. It is important to note that by increasing the width of the active area of the Opto-VLSI processor to 19 mm, the number of the output fiber ports can be as high as 32, making the adaptive OPS an attractive product for access optical networks and optical signal processing.

Acknowledgment

The authors would like to acknowledge the support of the Faculty of Health, Engineering, and Science, Edith Cowan University.

References

[1] W. Liu, Y. Zeng, C. Long, L. Yong, and K. Wu. (2005, Mar.). Variable optical power splitters create new apps. *Lightwave.* [Online]. vol. 22, no. 3, p. 11. Available: http://www.lightwaveonline.com/articles/print/volume-22/issue-3/technology/variable-optical-power-splitters-create-new-apps-53912057.html

[2] H. A. B. Mustafa, F. Xiao, and K. Alameh, "Photonic microwave filter employing an Opto-VLSI-based adaptive optical combiner," in *Proc. Int. Conf. HONET*, Riyadh, Saudi Arabia, Dec. 19–21, 2011, pp. 205–209.

[3] M. D. Vaughn, D. Kozischek, D. Meis, A. Boskovic, and A. Boskovic, "Value of reach-and-split ratio increase in FTTH access networks," *J. Lightwave Technol.*, vol. 22, no. 11, pp. 2617–2622, Nov. 2004.

[4] G. A. Queller. (2004, Jul.). Dynamic power distribution in PON/FTTP networks. *Lightwave.* [Online]. vol. 21, no. 7, p. 29. Available: http://www.lightwaveonline.com/about-us/lightwave-issue-archives/issue/dynamic-power-distribution-in-ponfttp-networks-53906787.html

[5] J. Shi and J. P. Fonseka, "Hierarchical self-healing rings," *IEEE/ACM Trans. Netw.*, vol. 3, no. 6, pp. 690–697, Dec. 1995.

[6] D. Griffith and S. Lee, "A 1 + 1 protection architecture for optical burst switched networks," *IEEE J. Sel. Areas Commun.*, vol. 21, no. 9, pp. 1384–1398, Nov. 2003.

[7] N. Kikuchi, Y. Shibata, H. Okamoto, Y. Kawaguchi, S. Oku, H. Ishii, Y. Yoshikuni, and Y. Tohmori, "Monolithically integrated 64-channel WDM channel selector with novel configuration," *Electron. Lett.*, vol. 38, no. 7, pp. 331–332, Mar. 2002.

[8] J. Capmany, B. Ortega, D. Pastor, and S. Sales, "Discrete-time optical processing of microwave signals," *J. Lightwave Technol.*, vol. 23, no. 2, pp. 702–723, Feb. 2005.

[9] J. Capmany, B. Ortega, and D. Pastor, "A tutorial on microwave photonic filters," *J. Lightwave Technol.*, vol. 24, no. 1, pp. 201–229, Jan. 2006.

[10] R. A. Minasian, K. E. Alameh, and E. H. W. Chan, "Photonics-based interference mitigation filters," *IEEE Trans. Microw. Theory Tech.*, vol. 49, no. 10, pp. 1894–1899, Oct. 2001.

[11] F. Xiao, B. Juswardy, and K. Alameh, "Tunable photonic microwave filters based on Opto-VLSI processors," *IEEE Photon. Technol. Lett*, vol. 21, no. 11, pp. 751–753, Jun. 2009.

[12] T. Sugiyama, M. Suzuki, and S. Kubota, "An integrated interference suppression scheme with an adaptive equalizer for digital satellite communication systems," *IEICE Trans. Commun.*, vol. E79-B, no. 2, pp. 191–196, Feb. 1996.

[13] H. A. B. Mustafa, X. Feng, and K. Alameh, "Opto-VLSI-based variable RF power splitter," in *Proc. 9th Int. Conf. HONET*, 2012, pp. 171–174.

[14] X. Zhao and S. Jose, "Dynamic power optical splitter," U.S. Patent 7 068 939 B2, Jun. 27, 2006.

[15] Z. Yun, L. Wen, C. Long, L. Yong, and X. Qingming, "A 1 × 2 variable optical splitter development," *J. Lightwave Technol.*, vol. 24, no. 3, pp. 1566–1570, Mar. 2006.

[16] F. Ratovelomanana, N. Vodjdani, A. Enard, G. Glasere, D. Rondi, and R. Blondeau, "Active lossless monolithic one-by-four splitters/combiners using optical gates on InP," *IEEE Photon. Technol. Lett.*, vol. 7, no. 5, pp. 511–513, May 1995.

[17] S. S. Choi, J. P. Donnelly, S. H. Groves, R. E. reeder, R. J. Bailey, P. J. Taylor, A. Napoleone, and W. D. Goodhue, "All-active InGaAsP-InP optical tapered-amplifier 1 × N power splitters," *IEEE Photon. Technol. Lett.*, vol. 12, no. 8, pp. 974–976, Aug. 2000.

[18] A. A. Ehsan, S. Shaari, and M. K. Abd Rahman, "Variable coupling ratio Y-branch plastic optical fiber (POF) coupler with suspended waveguide taper," *Progr. Electromagn. Res. C*, vol. 23, pp. 249–263, Nov. 2011.

[19] H. Kim, J. Kim, U.-C. Paek, B. H. Lee, and K. T. Kim, "Tunable photonic crystal fiber coupler based on a side-polishing technique," *Opt. Lett.*, vol. 29, no. 11, pp. 1194–1196, Jun. 2004.

[20] S-Y. Tseng, C. Fuentes-Hernandez, D. Owens, and B. Kippelen, "Variable splitting ratio 2 × 2 MMI couplers using multimode waveguide holograms," *Opt. Exp.*, vol. 15, no. 14, pp. 9015–9021, Jul. 2007.

[21] Q. H. Chen, W. G. Wu, Z. Q. Wang, G. Z. Yan, and Y. L. Hao, "Design and performance of MEMS multifunction optical device using a combined in-plane and out-of-plane motion of dual-slope mirror," *J. Lightwave Technol.*, vol. 28, no. 24, pp. 3589–3598, Dec. 2010.

[22] R. Zheng, Z. Wang, K. E. Alameh, and W. A. Crossland, "An opto-VLSI reconfigurable broad-band optical splitter," *IEEE Photon. Technol. Lett.*, vol. 17, no. 2, pp. 339–341, Feb. 2005.

[23] H. A. B. Mustafa, F. Xiao, and K. Alameh, "Adaptive optical splitter employing an Opto-VLSI processor and 4-*f* imaging system," *J. Lightwave Technol.*, vol. 28, no. 19, pp. 2761–2765, Oct. 2010.

[24] H. Mustafa, F. Xiao, and K. Alameh, "Reconfigurable optical power splitter/combiner based on Opto-VLSI processing," *Opt. Exp.*, vol. 19, no. 22, pp. 21 890–21 897, Oct. 2011.

[25] I. G. Manolis, T. D. Wilkinson, M. M. Redmond, and W. A. Crossland, "Reconfigurable multilevel phase holograms for optical switches," *IEEE Photon. Technol. Lett.*, vol. 14, no. 6, pp. 801–803, Jun. 2002.

[26] F. Xiao, K. Alameh, and T. T. Lee, "Opto-VLSI-based tunable single-mode fiber," *Opt. Exp.*, vol. 17, no. 21, pp. 18 676–18 680, Oct. 2009.

[27] S. T. Ahderom, M. Raisi, K. Alameh, and K. Eshraghian, "Testing and analysis of computer generated holograms for microphotonic devices," in *Proc. 2nd IEEE Int. Workshop DELTA*, Perth, Australia, Jan. 28–30, 2004, pp. 47–52.

[28] "Boulder nonlinear systems," in *1 × 4096 Liquid Multi-Level/Analog Liquid Crystal Spatial Light Modulator*. [Online]. Available: http://www.laser2000.de/fileadmin/Produktdaten/BNS/Datasheets/BNS-linear-4096.pdf